Fixed-Antenna Pointing-Angle Calibration of Airborne Doppler Cloud Radar

SAMUEL HAIMOV AND ALFRED RODI

Department of Atmospheric Sciences, University of Wyoming, Laramie, Wyoming

(Manuscript received 26 November 2012, in final form 9 April 2013)

ABSTRACT

Doppler velocity measurements from airborne meteorological Doppler radars require removal of the aircraft motion contribution in order to provide radial velocity of hydrometeor targets. This is a critical step for hydrometeor motion and wind retrievals. The aircraft motion contribution is defined as the scalar product between the radar antenna beam-pointing vector and the aircraft velocity vector at the antenna phase center. The accuracy in the removal of the aircraft velocity contribution is determined by the accuracy of the beam-pointing vector, the rigidity of the antenna mount, and the accuracy of the aircraft attitude and velocity measurements. In this paper an optimization technique is proposed to determine the antenna beam-pointing vector and to analyze its uncertainties using aircraft attitude and velocity data from a GPS-aided inertial measurement unit and radar observations of the earth surface. The technique is applied to Wyoming Cloud Radar (WCR) on the University of Wyoming King Air (UWKA) aircraft. The beam-pointing vectors of the two fixed downward-pointing WCR antennas are calibrated using data selected from several calibration flights. The maximum root-mean-square error in the calibrated beam-pointing angles is smaller than 0.03°, resulting in less than 0.1 $m s^{-1}$ aircraft motion residual error in the Doppler velocities after removing the aircraft motion contribution. Some applicability and limitations to other airborne Doppler radars with fixed antennas are discussed.

1. Introduction

Hydrometeor motion measurements and atmospheric wind estimation from airborne Doppler radars require removal of the aircraft motion contribution in the measured radar Doppler velocity. High-accuracy estimates of the pointing angles of the antennas and of aircraft attitude, velocity, and angular acceleration are needed for this correction.

The problem of estimating and correcting the antenna-pointing and navigational errors in airborne radar Doppler measurements has been addressed in several papers (Testud et al. 1995; Durden et al. 1999; Georgis et al. 2000; Bosart et al. 2002). Variational and optimization techniques have been proposed and the quality of the error corrections analyzed using the residual Doppler velocity of the radar returns from the earth surface. Durden et al. (1999) offer a recursive least squares procedure for Doppler velocity corrections without the use of navigational data. While this technique offers fairly crude corrections and has significant restrictions for its applicability, it could be a reasonable approach when navigational data for the radar-moving platform is not available. Testud et al. (1995) developed a variational procedure that provides correction factors related to the navigation, antenna mounting, radar positioning, and ranging errors. As originally proposed, the approach of Testud et al. requires data from flat and stationary surfaces. The mathematical problem is defined with seven equations and eight unknowns, where one of the unknowns (error in the known antenna tilt angle) was considered negligible. Later, Georgis et al. (2000) removed the restriction for flat surface by adding the use of digital elevation maps. Bosart et al. (2002) proposed an improvement of the error estimation in Testud et al. (1995) variational technique by applying an iterative procedure to further reduce the errors and account for the error in the antenna tilting angle. They also proposed the use of in situ measured wind at aircraft levels and dual-Doppler wind synthesis to prevent errors resulting from a violation of the stationarity of the earth surface. Their correction procedure is an elaborate optimization and statistical iterative

Corresponding author address: Samuel Haimov, University of Wyoming, Department 3038, 1000 E. University Ave., Laramie, WY 82071.
E-mail: haimov@uwyo.edu

DOI: 10.1175/JTECH-D-12-00262.1

process and requires the presence of appropriate weather and surface returns in the radar measurements. Also, as Bosart et al. (2002, p. 329) note, ''using a single set of correction factors for an entire flight'' could leave significant errors in some of the corrected data (greater than $1\,m\,s^{-1}$ in the aircraft ground speed and angular errors on the order of 1°). The authors point out that the main reason for this is a possible drift for some of the navigation data. The Testud et al. (1995) technique and its improved versions by Georgis et al. (2000) and Bosart et al. (2002) are intended primarily for airborne radars using mechanically spinning antenna(s), like the National Center for Atmospheric Research (NCAR) Electric Doppler Radar (ELDORA; NCAR 2012), for which errors in the antenna pointing due to the antenna rotation also have to be addressed and may require corrections for each flight.

In this paper, we propose a simpler and mathematically robust procedure that uses very accurate aircraft attitude, angular accelerations, and velocity data to provide a single set of beam-pointing calibration coefficients for fixed-mounted (nonrotating) antenna(s). Data from aircraft maneuvers flown over a relatively flat terrain are used in the calibration and the characterization of its uncertainty. The result is a set of antenna beam-pointing angles that are shown to be sufficiently constant for a radar deployment in a given field experiment. The aircraft motion is removed without a need for further corrections using surface and other data collected during research flights. This calibration has been developed for the Wyoming Cloud Radar (WCR) mounted on board the University of Wyoming King Air (UWKA) research aircraft (Haimov and Rodi 2012).

The UWKA is a modified Beechcraft Super King Air 200T equipped with in situ and remote sensing probes for studying atmospheric phenomena in the lower to midtroposphere (Wang et al. 2012; UWKA 2012). In the summer of 2011, the UWKA was equipped with a new high-precision geopositioning system (Trimble/Applanix, model POS AV410). It uses linear and angular acceleration measurements from an inertial measurement unit (IMU) and positioning data from Global Navigation Satellite Systems (GNSS). The AV410 GNSS antenna is mounted on the roof of the aircraft approximately 1.5 m from the IMU. The moment arm effect of the relative IMU-GNSS antenna location is corrected using surveyed locations with better than 0.05-m accuracy. In this study, we postprocessed IMU measurements with Trimble/Applanix POSPac software, implementing a tightly coupled Kalman filter for the IMU and GNSS data using dual L1/L2 frequency differential techniques. The manufacturer stated typical absolute and relative accuracy for this unit is shown in Table 1 (Applanix 2012).

TABLE 1. Trimble/Applanix AV410 airborne positioning system performance specifications including absolute accuracy for Standard Positioning System (SPS) and Extra Performance (XP) using dual L1/L2 differential frequency techniques. Relative accuracy drift means attitude will drift at this rate up to the maximum absolute accuracy.

Absolute accuracy	SPS	XP	Postprocessed
Position (m)	1.5–3.0	0.1–0.5	0.05–0.30
Velocity ($m\,s^{-1}$)	0.050	0.010	0.005
Roll and pitch (°)	0.020	0.015	0.008
True heading (°)	0.080	0.040	0.025
Relative accuracy			
Noise ($°\,h^{-0.5}$)		<0.1	
Drift ($°\,h^{-1}$)		0.50	

Wyoming Cloud Radar is a W-band (95 GHz, 3.16-mm wavelength) Doppler and polarimetric pulsed radar intended for airborne use on the University of Wyoming King Air research aircraft. It has also been fitted for installation on the National Science Foundation (NSF)'s NCAR C130 research aircraft. The radar has one transmitter and two receivers to handle dual-polarization signals. It is equipped with a fast switching (pulse by pulse) W-band circulator network, allowing the use of up to five single-polarization antennas. Currently, for the UWKA radar installation, there are four antennas (three single-polarization antennas and one dual-polarization antenna) pointing in different directions. More details about the radar characteristics can be found in Wang et al. (2012) and WCR (2012).

In this paper we focus on the beam-pointing calibration of the down and down–forward-pointing antennas (Fig. 1) mounted under the radar transceiver unit in a rigid cabinet inside the aircraft cabin. The two antennas are aligned along the aircraft longitudinal axis (Fig. 1, x axis), providing a plane sweep below the aircraft suitable for dual-Doppler wind retrieval (Damiani and Haimov 2006; Leon et al. 2006). The one-way half-power beamwidth of the down and the down–forward antennas are 0.5° and 0.6°, respectively. The down antenna is pointing about 3° aft from vertical, giving a near-nadir look for a straight and level flight. The down–forward antenna is pointing roughly 26° off of vertical toward the nose of the aircraft, providing close to 30° separation between the two antenna-pointing directions. The radar is located about 3 m aft from the IMU. The altitude ceiling for the UWKA is about 9 km, and the maximum useable radar range is less than 15 km. The earth curvature at these distances is negligible and is ignored in this analysis.

In the following sections, we formulate the calibration problem and describe the calibration procedure and the necessary flight maneuvers. Flight data are then used to

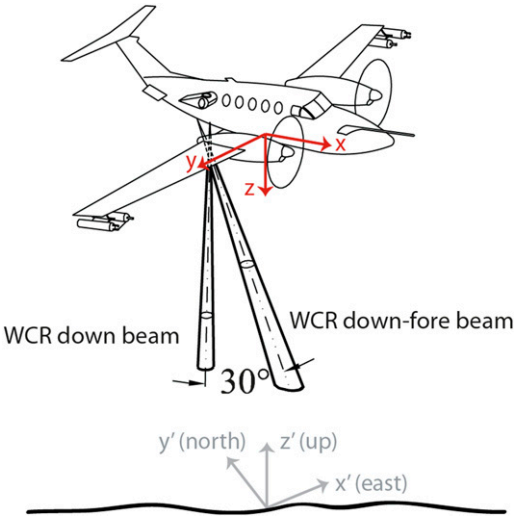

FIG. 1. Schematic presentation of the WCR two down-pointing antenna beams on the UWKA and the coordinate systems utilized in their calibration. For legibility the earth coordinate system is shown at the ground just below the aircraft, while its origin is the same as the origin of the aircraft coordinate system— i.e., the two coordinate systems are related to each other by a rotation transformation matrix only; there is no translation (see the text).

determine the beam angles and analyze their uncertainties. Both simulation and test flight data are used to evaluate the results of the calibration. Finally, the beam angle calibration is evaluated with more than 50 h of data from research flights during a recent field campaign.

2. Calibration problem formulation

Doppler velocity from a radar-illuminated volume (range gate) can be expressed as the scalar product $v = \mathbf{b} \cdot (\mathbf{V}_s + \mathbf{V}_p)$, where $\mathbf{b} = (b_x, b_y, b_z)$ is the unit vector of the radar beam-pointing vector ($|\mathbf{b}| = \sqrt{b_x^2 + b_y^2 + b_z^2} = 1$), $\mathbf{V}_s$ is the mean three-dimensional (3D) velocity vector of the scatterers within the range gate, and $\mathbf{V}_p = (V_{px}, V_{py}, V_{pz})$ is the 3D velocity vector of the radar platform motion at the radar antenna; v is the reflectivity-weighted mean target velocity along the radar beam and relative to the radar platform. Positive velocity means motion toward the radar. The reference coordinate system for the above-mentioned vectors is the aircraft reference system (ACRS) $Oxyz$ (see Fig. 1). It is a Cartesian coordinate system with origin O located at the sensing point of the aircraft IMU, x is parallel to the aircraft longitudinal axis, y is parallel to the aircraft right wing, and z is pointing down. For the fixed earth ground reference system (FGRS) $O'x'y'z'$, origin O' coincides with the origin O of the ACRS, x' is east, y' is north, and z' is up. The representation of the vectors described above in ACRS and FGRS is uniquely defined by a transformation matrix determined by a series of rotations (Wendisch and Brenguier 2013): 1) rotate by roll angle φ (right wing down positive) to wings horizontal around body x axis; 2) rotate by pitch angle θ (nose up positive) to x axis horizontal about body y axis; and 3) rotate by heading ψ (true heading, positive from north toward east) about z axis to north. Note that the ACRS origin is fixed with the FGRS origin (ACRS is not moving with respect to FGRS) and the transformation matrix represents the rotation (change in attitude) only; there is no translation. In other words, contrary to the intuitive thinking, the aircraft velocity vector defined in ACRS represents the earth relative velocity in the aircraft coordinate system. The transformation from FGRS to ACRS is similar to that shown in Wendisch and Brenguier (2013), except that we are using an east–north-up instead of north–east-down FGRS, and is given by

$$\mathbf{T} = \begin{pmatrix} t_{11} & t_{12} & t_{13} \\ t_{21} & t_{22} & t_{23} \\ t_{31} & t_{32} & t_{33} \end{pmatrix} = \begin{pmatrix} \sin\psi\cos\theta & \cos\psi\cos\phi + \sin\psi\sin\psi\sin\phi & -\cos\psi\sin\phi + \sin\psi\sin\theta\cos\phi \\ \cos\psi\cos\theta & -\sin\psi\cos\phi + \cos\psi\sin\theta\sin\phi & \sin\psi\sin\phi + \cos\psi\sin\theta\cos\phi \\ \sin\theta & -\cos\theta\sin\phi & -\cos\theta\cos\phi \end{pmatrix}.$$

The aircraft velocity vector is $\mathbf{V}_a = \mathbf{V}_{a'}\mathbf{T}$, where $\mathbf{V}_a = (V_{ax}, V_{ay}, V_{az})$ is in ACRS, $\mathbf{V}_{a'} = (V_{\rm ew}, V_{\rm ns}, V_w)$ is the aircraft velocity vector with respect to FGRS, $V_{\rm ew}$ is the east component, $V_{\rm ns}$ is the north component, and V_w is the vertical component of the aircraft ground velocity; $\mathbf{T}$ is orthogonal and therefore the inverse transformation, from ACRS to FGRS, requires only a transposition of $\mathbf{T}$ (e.g., $\mathbf{V}_{a'} = \mathbf{V}_a\mathbf{T}'$, where $\mathbf{T}'$ is the transpose of $\mathbf{T}$).

For a nonzero distance between the IMU (ACRS origin) and the radar antenna, the aircraft rotational velocity $\boldsymbol{\omega} = (\omega_x, \omega_y, \omega_z)$ contributes to the aircraft velocity in the beam $\mathbf{V}_p$. If the connecting structure between the IMU and the antenna is rigid and does not flex and twist, then the apparent radar platform velocity vector $\mathbf{V}_p$ can be written as $\mathbf{V}_p = \mathbf{V}_a + \boldsymbol{\omega} \times \mathbf{R}$. The $\boldsymbol{\omega} \times \mathbf{R}$ component is commonly referred to as radar-arm moment contribution. The aircraft velocity vector $\mathbf{V}_a$, aircraft rotational velocity vector $\boldsymbol{\omega}$, and the arm distance vector $\mathbf{R} = (R_x, R_y, R_z)$ between the IMU and the radar antenna are all with respect to ACRS.

The AV410 GNSS/IMU outputs aircraft attitude angles (roll, pitch, and true heading), $\boldsymbol{\omega}$ (aircraft body axes—roll rate, pitch rate, and yaw rate), and the ground-referenced aircraft velocity vector $\mathbf{V}_{a'}$. Using the transformation matrix $\mathbf{T}$ and the quantities defined above, the radar-measured Doppler velocity for a given range gate can be written as

$$v = \mathbf{b} \cdot (\mathbf{V}_s + \mathbf{V}_{a'}\mathbf{T} + \boldsymbol{\omega} \times \mathbf{R}).$$

When the radar Doppler measurement is from a range gate containing a return from a stationary surface only, $\mathbf{V}_s = 0$ and the above equation becomes

$$v = \mathbf{b} \cdot (\mathbf{V}_{a'}\mathbf{T} + \boldsymbol{\omega} \times \mathbf{R}). \quad (1)$$

The unknowns in (1) are the beam-pointing vector $\mathbf{b}$ and the radar-arm moment distance vector $\mathbf{R}$. The distance vector can be measured accurately and is constant for any specific radar installation. Given many independent Doppler measurements from the ground, the scalar form of (1) represents an overdetermined linear system with three unknowns (b_x, b_y, and b_z) and a nonlinear constraint, $\sqrt{b_x^2 + b_y^2 + b_z^2} = 1$. The nonlinear system that has to be solved for $\mathbf{b}$ can be written as

$$V_{px}^i b_x + V_{py}^i b_y + V_{pz}^i b_z = v^i, \quad i = 1, 2, \ldots, N \quad \text{and} \quad (2a)$$

$$\sqrt{b_x^2 + b_y^2 + b_z^2} = 1, \quad (2b)$$

where N is the number of measurements and the system coefficients V_{px}, V_{py}, and V_{pz} for each measurement i are given by

$$\begin{aligned} V_{px} &= t_{11}V_{\text{ew}} + t_{12}V_{\text{ns}} + t_{13}V_w + V_{\text{R1}}; \quad V_{\text{R1}} = R_z\omega_y - R_y\omega_z, \\ V_{py} &= t_{21}V_{\text{ew}} + t_{22}V_{\text{ns}} + t_{23}V_w + V_{\text{R2}}; \quad V_{\text{R2}} = R_x\omega_z - R_z\omega_x, \quad \text{and} \\ V_{pz} &= t_{31}V_{\text{ew}} + t_{32}V_{\text{ns}} + t_{33}V_w + V_{\text{R3}}; \quad V_{\text{R3}} = R_y\omega_x - R_x\omega_y, \end{aligned}$$

where V_{R1}, V_{R2}, and V_{R3} are the velocity contributions due to the radar-arm moment. The system (2) defines the beam calibration problem in ACRS.

Note that if $\boldsymbol{\omega}$ (and/or $\mathbf{R}$) is zero (aircraft angular acceleration is negligible and/or the IMU is located in a very close proximity to the radar antenna phase center and therefore $V_{\text{R1}} = V_{\text{R2}} = V_{\text{R3}} = 0$), then the expressions for the coefficients V_{px}, V_{py}, and V_{pz} are the same regardless of which reference frame, ACRS or FGRS, is used. This follows from the equality $(\mathbf{b}\mathbf{T}') \cdot \mathbf{V}_{a'} = \mathbf{b} \cdot \mathbf{V}_a$. However, this is not the case when the radar-arm moment contribution is nonzero, that is, $\mathbf{V}_R = (V_{\text{R1}}, V_{\text{R2}}, V_{\text{R3}}) \neq 0$. The expressions for V_{R1}, V_{R2}, and V_{R3} in ACRS are simple linear functions of the aircraft body axis accelerations, as shown above. If the beam calibration problem (2) is derived in the FGRS, then $\mathbf{V}_R$ is a more complex nonlinear function of the aircraft attitude and rotational rates, $(\boldsymbol{\omega} \times \mathbf{R})\mathbf{T}'$, and so are the expressions for V_{px}, V_{py}, and V_{pz}. Therefore, to the extent that there is a noise component in the aircraft attitude and acceleration measurements, solving the beam calibration problem (2) in ACRS is preferable.

3. Calibration procedure

The calibration procedure is organized into three steps: (i) radar surface return data are collected from several calibration flights; (ii) the data are divided into independent data segments (calibration legs), and for each calibration leg a numerical optimization procedure is run to solve the system (2); and (iii) a statistical analysis is performed to establish the beam-pointing calibration coefficients and their uncertainty.

a. Aircraft beam calibration maneuvers, environment and target conditions, and radar parameters

Aircraft radar beam calibration maneuvers are designed to enhance the aircraft motion contribution into the radar antenna beam with respect to the three ACRS axes and thus increase the robustness of the solution of (2). The maneuvers include aircraft attitude angle variations typically encountered in research flight patterns. They are also designed to provide strong and unperturbed returns from ground.

The calibration legs consist of short (approximately 2 min) straight and level legs with different angles between the aircraft heading and the mean wind direction and varying aircraft sideslip angle $\beta = \tan^{-1}(V_{ay}/V_{ax})$, straight legs with strong crosswind, ramps with different pitch angle, and pairs of two right-turn and two left-turn circles with roll angles between 30° and 45° (see flight pattern shown in Fig. 3). The typical average flight altitude for a constant-level calibration leg is in the vicinity of 1000 m above ground level (AGL). For maneuvers with changing altitude, the minimum altitude is about 500 m AGL and the maximum near 4000 m AGL. Also,

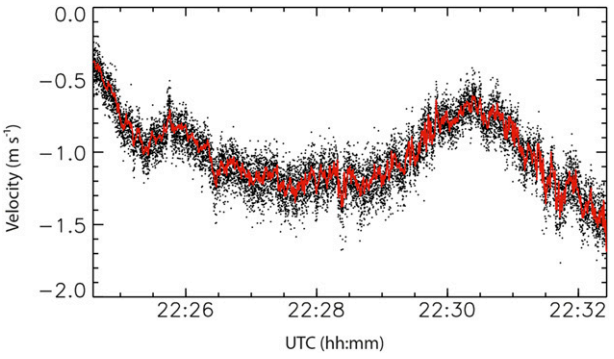

FIG. 2. Aircraft velocity vector contribution to the radar down-pointing antenna measurements (solid red line) and the radar Doppler measurements of the ground range gate velocity (black dots). Data segment is from the 5 Dec 2011 calibration flight.

straight ascending and descending (ramp) legs up to 8000 m MSL and level legs at 3000–4000 m MSL under different cabin pressure are performed to test the effect of the cabin pressurization on the antenna orientation due to fuselage flexing. In addition, maneuvers are performed that simulate more extreme turbulence conditions encountered during research flights. They are used to test the calibration precision when the aircraft frame is subject to increased stress and rapid and/or steep changes in the aircraft attitude and accelerations are present, all within the specified certification limits of the aircraft.

The calibration flights should be in clear air or at most weak clouds without precipitation. The terrain illuminated by the radar should be reasonably flat without lakes, blowing snow or dust, moving targets on the ground, or in the air close to the ground. The flatness of the terrain and the avoidance of lakes/ponds allows for steadier signal-to-noise ratio (SNR) of the surface return and more accurate estimation of the ground gate. The type of ground (bare, low-height vegetation, wooded, etc.) and the strength of the surface winds affect the surface return Doppler velocity spread. Terrains with plowed agricultural lots or low-height vegetation are optimal. Light to moderate winds at flight levels are preferred, since they are sufficient to decorrelate the velocity measurements in time and provide independent samples of the aircraft motion contribution into the beam, generating a well-conditioned system (2).

For these flights, the radar-transmitted pulse was set to 200 ns and the radar-received signal was sampled every 7.5 m in range. Given the altitude and attitude of the aircraft during the calibration legs and the narrow beamwidth of the antennas, the ground return signal is mainly beam limited. With oversampling the pulse by a factor of 4, it is straightforward to determine accurately the surface gate based on the received power. In section 4, the surface ranging error using high-resolution digital elevation map (DEM) is analyzed. The along flight path radar sampling is approximately every 3–5 m, depending on the radar dwell time and the aircraft speed. The pulse repetition interval is set to 50 μs [pulse repetition frequencey (PRF)] of 20 kHz, resulting in a maximum unambiguous velocity range of $\pm 15.8\,\mathrm{m\,s^{-1}}$.

b. Data measurement errors

The measurement errors present in the coefficients V^i_{px}, V^i_{py}, V^i_{pz}, and v^i can be grouped as GNSS/IMU errors in $\mathbf{V}_{a'}$, $\mathbf{T}$, and $\boldsymbol{\omega}$, arm error in $\mathbf{R}$, and noise and interferences in the radar-measured Doppler velocity v of the ground. One example of the radar down-pointing antenna-measured v and the aircraft velocity vector contribution to that antenna, $\mathbf{b} \cdot \mathbf{V}_p$, is shown in Fig. 2, where the solid red line is the aircraft velocity contribution and the black dots are the radar Doppler measurements of the ground return. The radar measurements are noisier than the aircraft GNSS/IMU measurements.

The radar Doppler measurements are affected by the radar system noise because of the finite SNR. The typical SNR for the calibration data is greater than +30 dB, and therefore the radar system noise adds little to the uncertainty in the measured Doppler of the ground returns. Another contribution to the uncertainty in the Doppler velocities is a result of the Doppler spectrum broadening because of the aircraft fast-forward motion and the antenna finite beamwidth (Skolnik 2008, p. 3.9). For the antennas and the data we use in this analysis, the additional uncertainty in v, caused by broadening, after averaging, is a few centimeters per second. There is an additional random error caused by the broadening of the surface return Doppler spectrum depending on the type of surface and the environmental conditions (e.g., surface wind). For the surface and the environmental conditions during the calibration data measurements, this error is small as well (Barton and Ward 1984, p. 139). Other possible transient contributions to v that are not accounted for in the left side of (2a) are changes in the radar antenna mounting orientation resulting from fuselage flexing and expansion during a flight or other undetermined causes. For an aircraft speed of $100\,\mathrm{m\,s^{-1}}$, a change of 0.1° in the antenna pointing in the direction of the aircraft velocity vector causes close to $0.2\,\mathrm{m\,s^{-1}}$ aircraft motion contribution to the measured radial Doppler velocity. A change in the fixed antenna mounting may be due to accelerations caused by (i) aircraft maneuvering, (ii) strong turbulence, and (iii) large changes in pressure differential between cabin and outside. These effects could result in a small temporary change in the antenna-pointing angles that are difficult to quantify and may lead to biases and random errors. Given the high-precision GNSS/IMU, we ignore the errors in the

aircraft navigational data. These errors, to the extent they are not completely negligible, will contribute to the uncertainty in the calibrated beam-pointing angles and the residual velocity of the ground.

Numerical/rounding errors associated with the solver of the system (2) are minimal—all critical calculations are done in double precision. However, the noise in the measurement data as well as the level of independence of the measurements may affect the correctness of the solution.

In the following sections, we examine these errors as they pertain to the UWKA installation of the WCR and the actual calibration data used.

c. Calibration data and calibration calculations

Seven hours of radar surface return data from six calibration flights on 3 November and 5 December 2011, 3 and 5 January, 8 March, and 6 April 2012 were collected. The calibration legs were flown over southeastern Wyoming with an average elevation of 1500–2200 m and changes in the elevation of less than 100 m per leg. The area was covered primarily with low-height vegetation and snow for some of the flights. A Google Earth view of the terrain and the flight track for the 3 November 2011 calibration flight providing half of the calibration legs are shown in Fig. 3. After examining the data, 44 calibration legs are selected with a combined duration of 1 h and 54 min, representing on average about 4000 independent surface measurements per calibration leg (at the UWKA research speed of about 90 m s^{-1}). Table 2 shows some of the parameters for the calibration legs combined by type.

The calibration calculations involve solving the nonlinear system (2) for each calibration leg. The left side of system (2) includes second-order nonlinearity and is affected by small GNSS/IMU errors. The GNSS/IMU errors have a weak effect on the system coefficients (V^i_{px}, V^i_{py}, and V^i_{pz}). A simulation analysis (not shown) assuming 0.1° rms error in attitude and accelerations results in approximately 0.2 m s^{-1} uncertainty in V^i_{px}, V^i_{py}, and V^i_{pz}. In our calibration we utilize the AV410 post-processed data for which the manufacturer stated angular rms errors are 4–8 times smaller.

The right side of the system is the measured Doppler surface velocity by the radar. This is the main source of random errors (see Fig. 2). In addition, transient flexing of the fuselage may cause a temporary change in the antenna pointing that is not accounted for by the radar-arm moment component and thus generating a bias in the Doppler velocity of the surface. While this is not actually a measurement error, it may not be possible to correct for such an effect to the solution's uncertainty and bias.

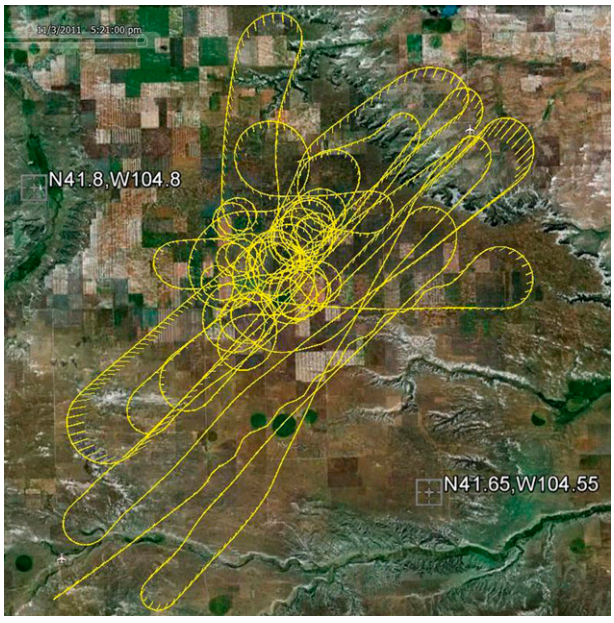

FIG. 3. Terrain map of a southeastern Wyoming area overflown by UWKA during the 3 Nov 2011 calibration flight. The flight track between 1520 and 1720 UTC is shown in yellow.

The problem (2) can be solved using nonlinear least squares methods or optimization (minimization) techniques. Most scientific computation software packages provide routines to solve (2) using either approach. We tested several routines (lsqnonlin and fsolve from MATLAB and constrained_min from IDL), and they all deliver nearly the same solutions. We also tested the sensitivity of the solution under different minimization (cost) functions. The results were similar and a least squares minimization technique was used for this paper. In the next section, we discuss the calibration results and the associated uncertainties.

4. Analysis of the beam-pointing calibration results

a. Calibration coefficients and their uncertainty

The results for b_x, b_y, and b_z from the solver of (2) for all 44 calibration legs are shown in Fig. 4. The three left-hand panels are for the down antenna and the three right-hand panels are for the down–forward antenna.

Any solution of (2) could include errors resulting from adverse perturbation in the Doppler measurements of the ground by moving targets, the optimization solution inaccuracies, and biases and uncertainty in the actual pointing direction caused by inflight distortions of the airframe. The histograms of the beam components shown in Fig. 4 are very narrow for the x and z components of the two beams—standard deviation of about 0.02° for the

TABLE 2. WCR beam-pointing calibration legs flown with the UWKA. Mixed leg type combines varying roll, pitch, and sideslip.

Leg type	No. of legs	Total duration (s)	Flight altitude (m)	Flight heading (°)	Wind ($m\,s^{-1}$)	Wind direction (°)	Aircraft sideslip (°)
1: Straight and level	6	1257	2500–2700	~50 and 230	4–14	220–250	−20 to +10
2: Straight and level	6	960	3000–3100	~130 and 310	7–18	190–230	<|1|
3: Ascending/descending ramp	3	545	2000–4100	40–240	4–16	200–280	+5 to +18
4: Two left/two right circles	18	2785	2500–3900	0–360	7–14	200–280	−18 to +12
5: Two left/two right circles	6	1012	3000–3900	0–360	14–27	270–290	<|1|
6: Mixed	5	807	2300–2900	0–360	3–14	215–250	−9 to +7

down beam and about 0.03° for the down–forward beam. The histograms for the y component of the beams are broad, with 0.14° and 0.18° standard deviations for the down and down–forward beams, respectively. There are also a few outliers in the x- and z-component histograms.

The broader distributions of the beams' y component are caused by the specific way the two down antennas are mounted. They are aligned in a vertical plane parallel to the aircraft longitudinal axis. Typical maximum values for the velocity component V_{py} do not exceed 5–10 $m\,s^{-1}$ for the calibration legs. For a deviation of b_y directional cosine by less than cos(0.5°) from cos(90°), the contribution of the V_{py} component of the platform motion into the beam would be less than 0.09 $m\,s^{-1}$. This is comparable to the noise in the Doppler measurements, and therefore it is to be expected that the solution for b_y would not be very accurate. The error in b_y can be reduced by using the best values of b_x and b_z, and calculate b_y from the norm of **b** (2b). Using this approach the uncertainty in b_y is reduced to about 0.03°. The values for b_y, shown as red lines in the middle panels of Fig. 3, are calculated using this approach, and they agree well with the areas of maximum frequencies in the histograms for b_y.

Ten outliers deviate more the 0.05° from the center of the main lobes in the histograms for b_x and b_z. Nine of

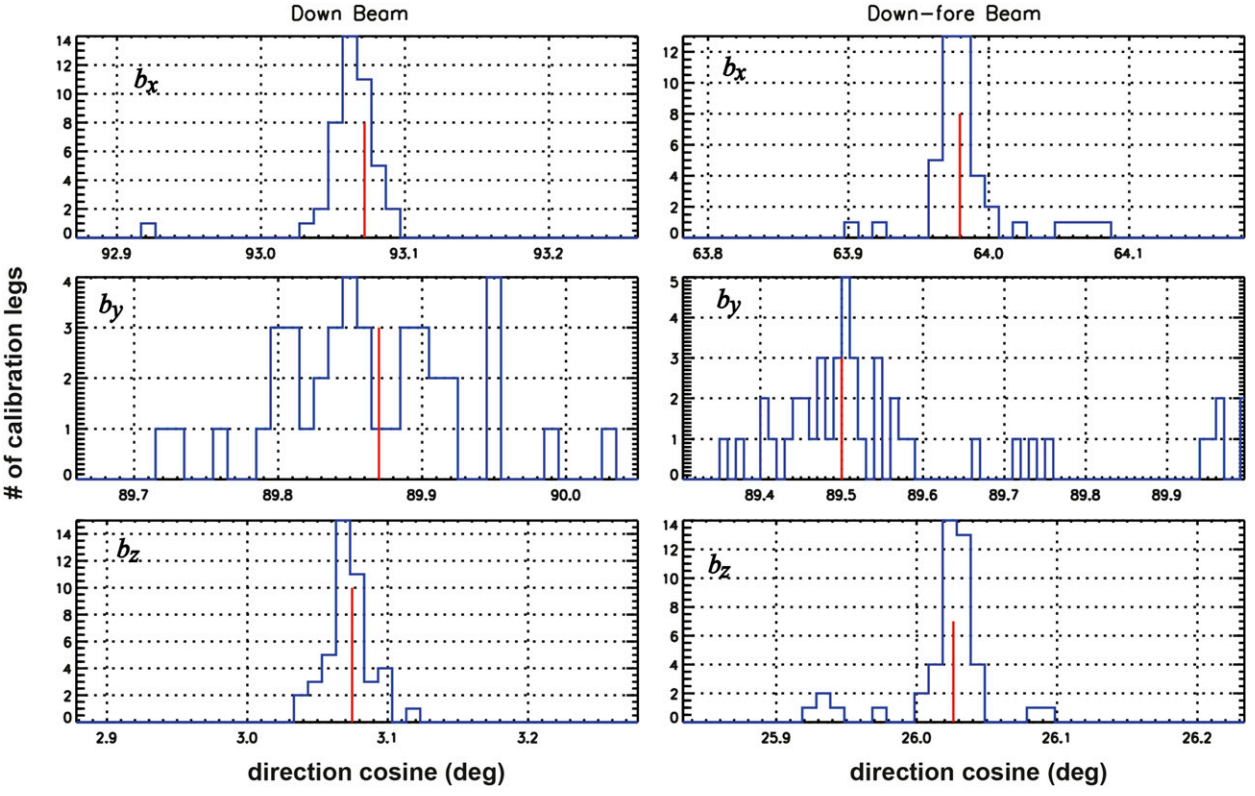

FIG. 4. Histograms of the antenna beam-pointing unit vector components b_x, b_y, and b_z for the WCR (left) down-pointing antenna and (right) down–forward-pointing antenna. The beam components are plotted as directional cosines in degrees. The red lines show the selected values for the final calibrated beam-pointing direction for both antennas.

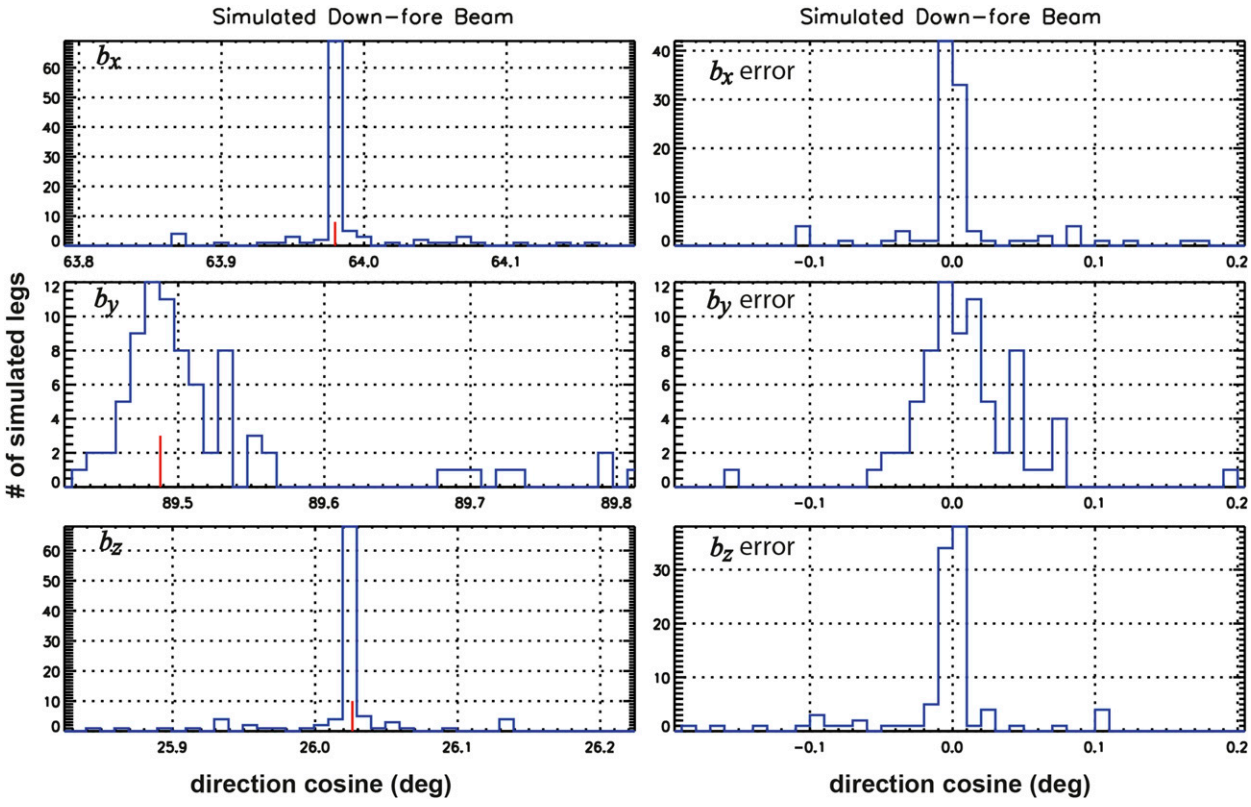

FIG. 5. (left) Down–forward antenna beam unit vector component histograms calculated from 102 simulated radar data segments with a known beam-pointing vector (short red lines) and platform motion contribution. (right) Histograms of the errors between the true beam vector and the calculated beam vectors.

them are generated by the solutions for straight flight calibration legs, eight of them flown in close alignment with the mean wind direction (leg type 1 in Table 2). In addition, the vertical air velocity variation for these legs is also small. Thus, the main contribution of the platform motion into the beams is mostly driven by the V_{ax}. To investigate this further, we ran a simulation analysis. Radar data from surface returns collected with the stationary WCR (not in flight) are used as the baseline Doppler velocity signal not affected by aircraft motion. Gaussian noise is added to the stationary data to simulate the broadening of the Doppler spectrum caused by the finite beamwidth and the aircraft forward motion. The resultant mean Doppler velocity of these stationary measurements is $0.00\,\mathrm{m\,s^{-1}}$, and the standard deviation is about $0.05\,\mathrm{m\,s^{-1}}$. Then, actual aircraft motion as measured by the GNSS/IMU and corrected for the arm moment is added to the radar Doppler signal using the beam-pointing vector components, represented by the red lines in Fig. 4. Assembled in such a way, this signal simulates the Doppler velocity of the radar return from the earth surface while in flight, but without added uncertainty resulting from unaccounted motion perturbations in the beam from the ground target and the flexing of the aircraft airframe. The data from the flight also include the straight legs that contain the outlier solutions mentioned above. A total of 137 min of flight data are used, of which, calibration legs of types 1–6 (Table 2) represent about half of the time; 102 simulated calibration legs are generated from this time series and the solutions for the system (2) are obtained.

Figure 5 shows the results of these simulation calculations for the down–forward beam vector components containing most of the outliers. Comparing Fig. 5 histograms in the left-hand panels with the corresponding ones from Fig. 4 right-hand panels shows that the distributions from the simulation are narrower but exhibit a similar fraction of outliers. All of the outliers are resulting from erroneous solutions of (2) caused by a weak contribution of the aircraft motion into the radar beam and poor decorrelation of V^i_{px}, V^i_{py}, and V^i_{pz} coefficients with time (i). The right-hand panels in Fig. 5 show the histograms of the errors between the 102 calculated beam vectors and the true beam vector used in the simulation. The errors larger than 0.05° in the x and z components are caused mostly by the legs that correspond to the straight

TABLE 3. WCR antenna beam-pointing unit vector in ACRS. The last column is the maximum beam-pointing angle error for one standard deviation error in b_x, b_y, and b_z.

	$\cos^{-1}b_x$ (°)		$\cos^{-1}b_y$ (°)		$\cos^{-1}b_z$ (°)		
WCR antenna pointing beam	Mean	Std dev	Mean	Std dev	Mean	Std dev	δ_b (°)
Down	93.072	0.011	89.870	0.017	3.075	0.013	0.021
Down–forward	63.979	0.008	89.488	0.011	26.026	0.008	0.016

legs aligned with the wind, including the ones that caused the outliers in Fig. 4. The same results hold for the down beam as well.

After excluding the unreliable straight legs, the final calibrated beam angles were determined by calculating the mean of the x and z components, and the b_y component was calculated from the norm of **b**. Additional fine-tuning of the down beam b_y component was done by using data from straight legs with strong crosswind (leg type 2 in Table 2). The resulting corrections of about 0.004° to **b** components were applied.

The mean angles and the standard deviations of the calibrated beam unit vector components are shown in Table 3. In addition, the maximum angle δ_b between the beam mean vector and a beam vector offset by one standard deviation in the vector components is calculated.

Analysis of the distributions of the calibration results for different types of calibration legs (not shown) supports the conclusion that it is sufficient to fly a large number of calibration circles (leg type 4) in order to obtain a similarly accurate estimate of the beam vector envelope. Furthermore, in Table 2 under leg types 5 and 6, a few pairs of circles with strong winds and more intense maneuvers are included. For these cases, at least for the UWKA, the results do not show statistically significant differences from the rest of the calibration legs.

An example of the achieved accuracy of the retrieved earth surface velocity using the calibrated beam vectors for the down- and down–forward antennas is shown in Fig. 6. Included in these are 12 left- and right-turn circles (three calibration legs) and two straight legs from the 3 November 2011 calibration flight as well as all data collected in between these legs. About half of the data in Fig. 6 are used in the determination of the beam unit vectors and the other half are used to demonstrate the consistency of the results. The mean ground velocity is within $\pm 0.03\,\mathrm{m\,s^{-1}}$, and the standard deviation is less than $0.08\,\mathrm{m\,s^{-1}}$. There is no significant difference in the

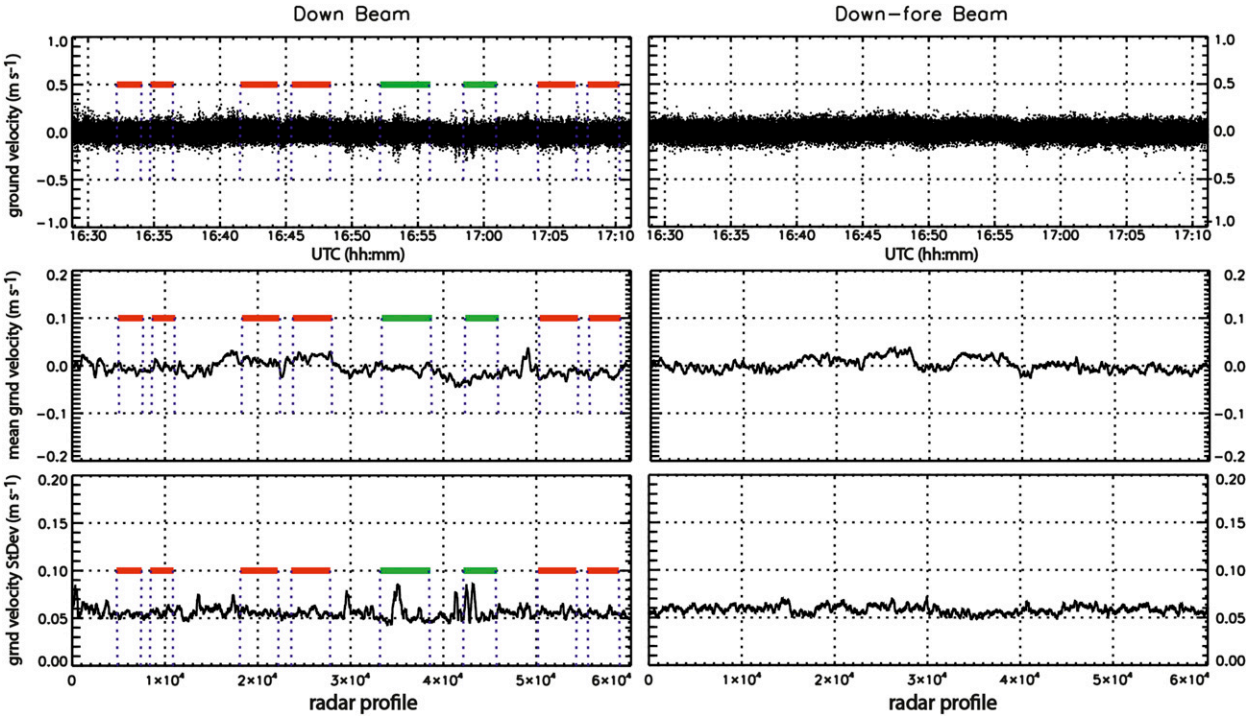

FIG. 6. Segment from the 3 Nov 2011 calibration flight. (top) Residual velocity of the ground, (middle) mean velocity of the ground, and (bottom) standard deviation of the ground velocity for the (left) down and (right) down–forward radar beams. The solid lines in (left) show the calibration legs (red for circles and green for straight legs). The calibration leg times are the same for the down and down–forward beams.

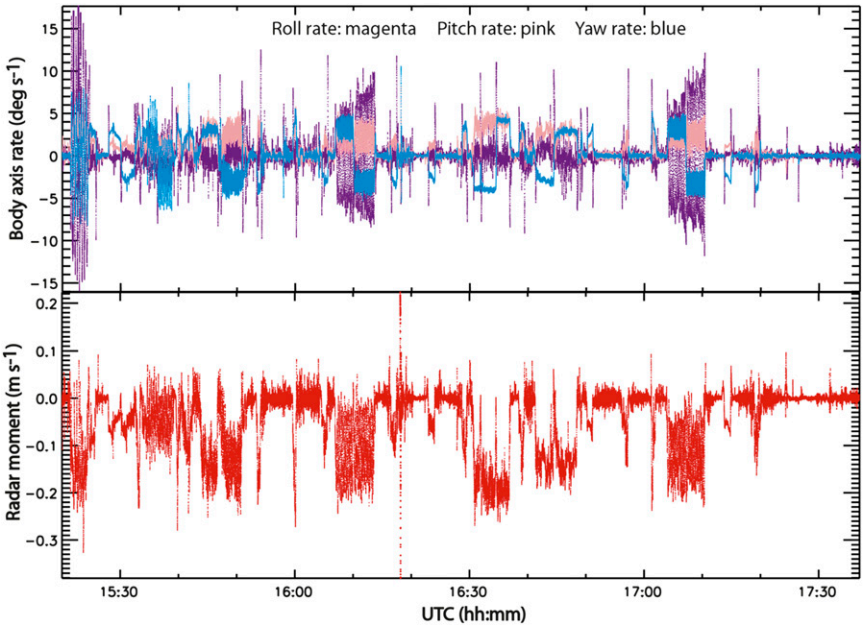

FIG. 7. (top) UWKA body axis accelerations measured by the GNSS/IMU for the 3 Nov 2011 flight, and (bottom) the corresponding radar–arm moment contribution to the WCR down antenna.

bias and the uncertainty between the calibration and the test data.

b. *Radar-arm moment contribution and radar-arm vector error*

The calibration system (2) accounts for the additional aircraft velocity contribution at the radar antenna due to the radar-arm moment. For the WCR down and down–forward antenna installations on UWKA, **R** is (−2.68, 0.01, −0.42) and (−3.08, −0.03, −0.33) meters, respectively. The absolute accuracy of these measurements is better than 0.05 m. Figure 7 shows time series of the calculated radar-arm moment contribution $\mathbf{b}\cdot(\boldsymbol{\omega}\times\mathbf{R})$ to the down beam. The magnitude of both the down and down–forward beam arm moment corrections is mostly less than 0.2 m s^{-1} for the calibration flight on 3 November 2011.

To analyze the sensitivity of the arm moment correction to errors in **R**, we used data from the 16 September 2011 flight, which had vigorous maneuvers. Figure 8 shows the arm moment contribution for the down–forward antenna and its error when assuming **R** has ±0.1 m error in each component. The magnitude of the radar-arm moment contribution during this flight reached 0.4 m s^{-1}—considerably in excess of a normal research flight. Even under such extreme conditions, a 0.1-m error in **R** causes a less than 0.02 m s^{-1} error in the radar-arm moment. The down antenna distance vector error showed similar sensitivity.

c. *Ground return range gate error*

In the calibration procedure, we used the maximum return power as an identifier of the range gate, providing the Doppler measurement of the surface for all calibration legs. Here we examine the accuracy of this approach. For all calibration legs, we use the calibrated beam-pointing vector as defined above and the one arc second global DEM data from the Advanced Spaceborne Thermal Emission and Reflection Radiometer (ASTER) database (ASTER 2012) to determine the surface range gate independent on the radar-received power. The absolute vertical accuracy of the ASTER data may vary and depends on several factors, but over the area we conducted the calibration flights the accuracy is estimated to be no worse than 10–15 m, which is close to the 7.5-m sampling in range for the radar data. This leads roughly to a two range gate uncertainty in finding the radar surface gate using the DEM. One example comparing the surface gate determined from the calibrated beam angles and the ASTER data with the gate identified by the maximum radar-received power is shown in Fig. 9; the data being the same as in the Fig. 6 case. The terrain under the calibration legs is flat within a 30-m change in elevation. In between the legs, there is up to about a 200-m deviation in elevation with terrain mean local slopes of less than 3°.

Given the uncertainties in the DEM and the error resulting from the finite radar range sampling, the match

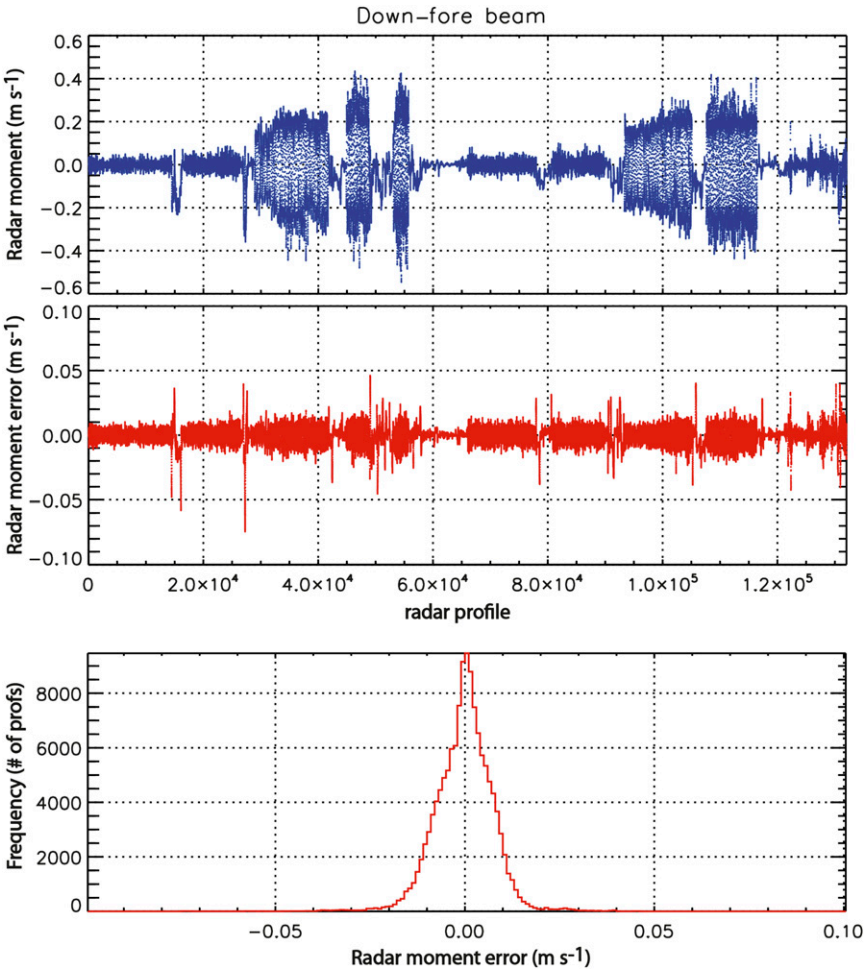

FIG. 8. (top) Radar–arm moment contribution for the down–forward antenna from the 16 Sep 2011 flight. (middle) Uncertainty in the radar–arm moment contribution from ±0.1 m error in **R**, and (bottom) the distribution of this error.

between the DEM-determined surface gates and the ones found with the maximum received power is excellent. Out of more than 60 000 radar profiles with surface returns, 0.4% for the down beam and 1.3% for the down–forward beam are showing a difference of more than 15 m. We have made a similar comparison for data from mountain terrain with a change in elevation of more than 1000 m and slopes exceeding 10°, and the results are also very good.

5. Calibration evaluation

The calibrated down and down–forward antenna beam unit vectors given in Table 3 are tested using all the surface data from the calibration flights. The weather conditions for these flights are near optimal. The largest uncertainty in the variability of the Doppler velocity measurements of the surface comes from possible nonoptimal surface conditions, mainly from surface data outside the calibration areas. Figure 10 shows the distributions of the residual velocity of the surface from the entire dataset, 27% of which was used in the beam determination. Data from more than 5 h of flying time are included, providing around 350 000 radar profiles with surface returns. The mean velocity of the ground is within $\pm 0.01\ \mathrm{m\,s^{-1}}$, and the standard deviation is less than $0.1\ \mathrm{m\,s^{-1}}$. These results are comparable to the mean and the standard deviation calculated for each of the calibration legs. However, the tails in the distributions shown in Fig. 10 extend to larger values. Ground velocity exceeding $0.2\ \mathrm{m\,s^{-1}}$ is present in 3% of the data for the down beam and 4.5% of the data for the down–forward beam. In comparison, for the example shown in Fig. 6, these percentages are 0.3% and 0.1%, respectively. There are also 31 (0.008%) surface velocity points for the down beam (and 98 for the down–forward beam) that exceed $0.5\ \mathrm{m\,s^{-1}}$ in magnitude. The

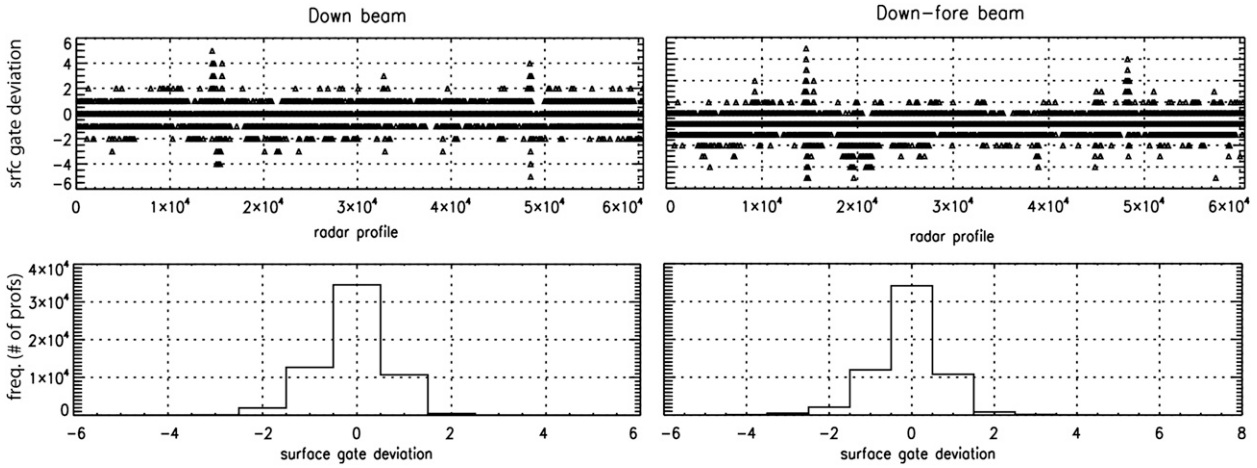

FIG. 9. (top) Difference between radar surface gates found using the DEM data and the calibrated beam unit vectors and the surface gates determined by the radar maximum received power for the (left) down and (right) down–forward beams. (bottom) Distributions of the surface gate deviations. One gate is equal to 7.5 m.

aircraft attitude and the weather conditions for both datasets are similar. However, most of the flying beyond the calibration legs is transitioning from one leg to another and ferrying to and from the calibration sites, which frequently placed the aircraft outside of the area selected for calibration. We believe that a significant number of the data points in the Fig. 10 distribution exceeding $0.2\,\mathrm{m\,s^{-1}}$ are caused by events not associated with increased bias and uncertainty in the beam angles, but by external contribution to the Doppler return from the surface. Using the UWKA high-definition downward-pointing video camera, we examined some individual cases where the velocity of the ground deviated more than $0.5\,\mathrm{m\,s^{-1}}$ and found that a moving train and ranch/farm small wind mill could cause a Doppler bias of 0.2–$0.8\,\mathrm{m\,s^{-1}}$ as well as increased standard deviation.

High pressure differential between the cabin pressure and the outside air pressure could cause airframe flexing

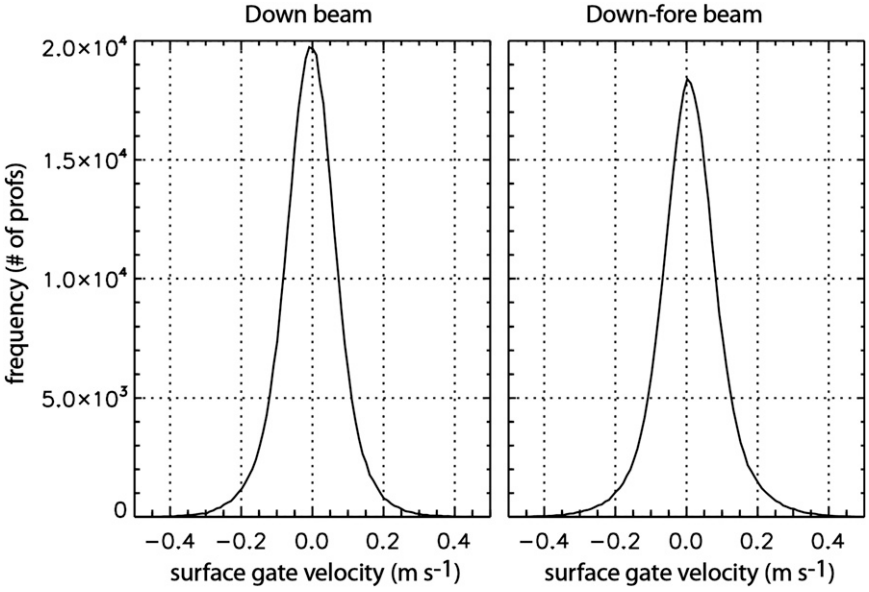

FIG. 10. Distribution of the radar Doppler velocity of the surface for the (left) down-pointing beam and (right) down–forward-pointing beam. The mean (std dev) of the velocity is −0.006 (0.08) and 0.010 (0.09) $\mathrm{m\,s^{-1}}$ for the down and down–forward beam, respectively. The total number of radar profiles containing surface returns is 356 082 (346 354) for the down (down–forward) beam.

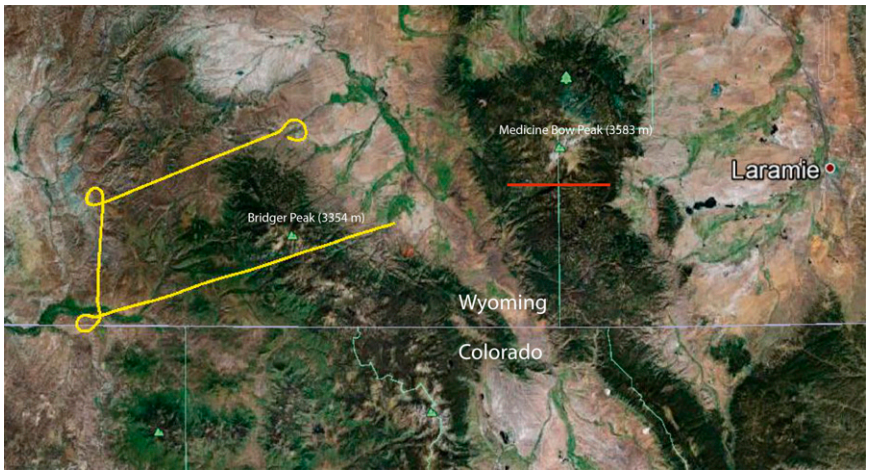

FIG. 11. Terrain map and UWKA flight track (yellow line) for a flight segment during 9 Jan 2012 ASCII flight. The red line is the UWKA flight track for the data segment shown in Fig. 13.

that may change the antenna-pointing angle. The maximum cabin pressure differential for UWKA is about 420 hPa. During the calibration flights, the cabin pressure varied between about 750 and 800 hPa, while the external pressure was from 610 to 800 hPa with most of the calibration data taken at air pressures of 700–780 hPa. Pressure differentials of less than 240–270 hPa do not appear to affect noticeably the antennas pointing and therefore the calibration results do not account for this effect. To examine the pressure effect, flight legs under different pressure differentials and flying conditions were performed: (i) a series of straight and level flight legs at constant altitude and different cabin pressure, (ii) straight and level flight legs at low altitude and high altitude with the typical cabin pressure used during research flights, and (iii) ascending and descending straight ramps from about 3000 to 8000 m MSL while maintaining constant cabin pressure equivalent to about 2000 m MSL. For all legs the Doppler velocity of the surface after correcting for the aircraft motion contribution using the calibrated beam-pointing vectors were analyzed. The highest pressure differentials for flight legs of (i) and (ii) caused up to $0.05\,\mathrm{m\,s^{-1}}$ mean bias, but fluctuations in the bias were almost of the same order. The bias is more significant for the flight legs of (iii), where it reached close to $0.1\,\mathrm{m\,s^{-1}}$ for the down beam and exceeded $0.1\,\mathrm{m\,s^{-1}}$ for the down–forward beam at pressure differentials near 400 hPa, although even in these cases the bias was not very consistent. More data are needed in order to establish if a correction could be applied in order to compensate for the cabin pressurization on the antenna pointing. In any case, the mean absolute bias was found to be typically less than $0.1\,\mathrm{m\,s^{-1}}$ and more apparent when the aircraft is ascending or descending at large pressure differentials. The majority of the UWKA research flying is below 7000 m MSL (23 000 feet), and the cabin pressure differential is rarely that large.

The antenna-pointing calibration coefficients obtained using the data from the calibration flights were used to correct the WCR Doppler data recorded during the Silver Iodide (AgI) Seeding Cloud Impact Investigation (ASCII) 2012 experiment. All flights for this experiment were flown over mountainous terrain. During ASCII, the WCR on board the UWKA was operated using a 250-ns pulse, 20-kHz PRF, 54-ms dwell time, and 15-m sampling in range.

The flight track for a clear-air segment on 9 January 2012 ASCII flight is shown in Fig. 11 (yellow line). From the terrain map it can be seen that the aircraft flew over some forest (mostly evergreens) and the rest of the area was largely covered with snow. The winds were light ($5–10\,\mathrm{m\,s^{-1}}$), the turbulence was low, and the aircraft roll angle during turns varied from $-40°$ to $+40°$. Figure 12 shows the residual velocity of the surface after removing the aircraft motion contribution using the calibration coefficients for the two down-pointing antennas given in Table 3. The bias and the uncertainty in the surface velocity are small and comparable to the results obtained from the calibration flights (see Fig. 6). A strong wind case ($15–30\,\mathrm{m\,s^{-1}}$ at flight level) during 18 January 2012 ASCII flight in clear air (not shown) and in the same area as the 9 January 2012 flight shows similarly small biases.

Most of the research flights during ASCII were in clouds and precipitation—light to heavy snow. We processed all of those flights in order to evaluate the effect of falling snow above the surface and stronger surface winds on the residual velocity of the ground measured by the radar after correcting for the aircraft motion

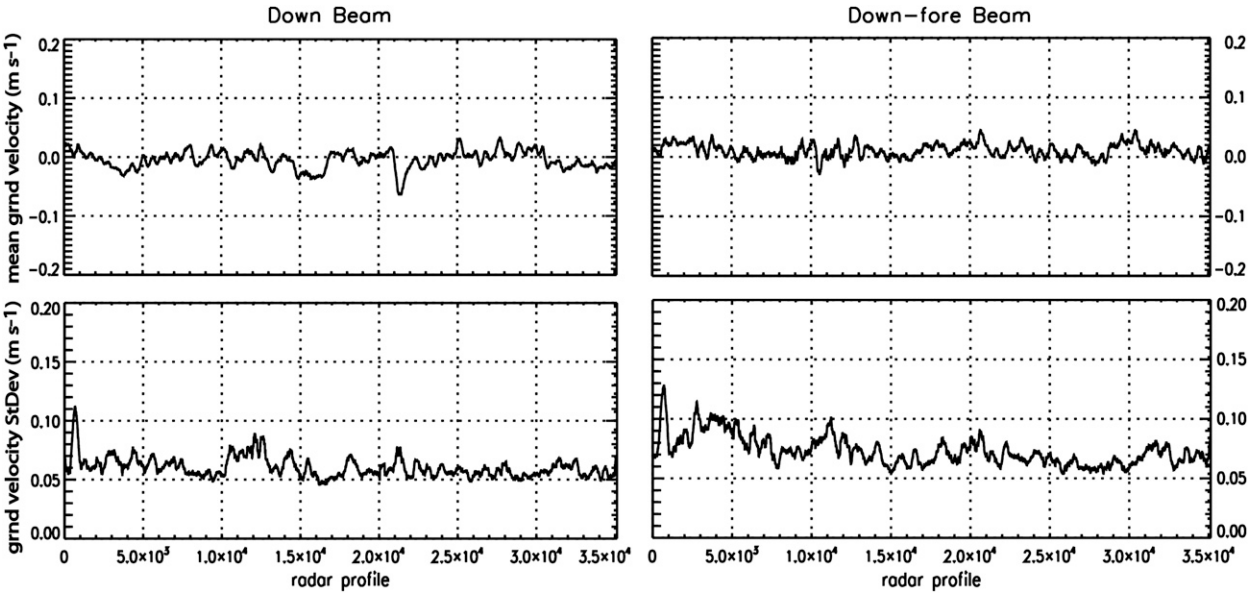

FIG. 12. Residual Doppler velocity of the radar ground return gates for the example shown in Fig. 11.

contribution. The effect is always small—bias rarely exceeding $0.1\,\mathrm{m\,s^{-1}}$ and standard deviation less than $0.2\,\mathrm{m\,s^{-1}}$. One factor responsible for the small error contribution in the ASCII surface velocity data is the lower than −20 dB hydrometeor-to-ground power ratio as well as the typically less than $10\,\mathrm{m\,s^{-1}}$ hydrometeor velocity in the surface gate resolution volume for the two down antennas. The detailed analysis of the bias and the uncertainty in the Doppler from the surface gate induced by weather targets is beyond the scope of this paper.

An example for a flight segment in clouds and snow precipitation from ASCII, recorded during the flight on 19 January 2012, is shown in Fig. 13. The top image is the WCR reflectivity and the bottom image is the corrected for aircraft motion contribution Doppler velocity from the down beam. The winds at flight level were westerly at 30–35 $\mathrm{m\,s^{-1}}$ and the aircraft was flying straight and level upwind. The flight track is shown as the short solid red line in Fig. 11. There is an apparent turbulent layer extending from the surface up to about 1 km AGL. The plotted velocities are ground-referenced motion of the hydrometeors (mostly ice), showing the fine structure in the hydrometeor velocity field. For this data segment, the mean residual velocity of the ground is $0.00\,\mathrm{m\,s^{-1}}$ and the standard deviation is $0.06\,\mathrm{m\,s^{-1}}$.

The error in the single Doppler radial velocity of the weather target, $\mathbf{b}\cdot\mathbf{V}_s$, assuming one standard deviation error in the beam-pointing angle, can be written as [Damiani and Haimov 2006, Eq. (13)]:

$$\varepsilon = [(\mathbf{b}_\varepsilon - \mathbf{b})\cdot\mathbf{V}_p + \mathbf{b}_\varepsilon\cdot\boldsymbol{\varepsilon}_p] + k_{s,c}r\delta_b, \qquad (3)$$

where $\mathbf{b}$ is the true beam-pointing unit vector, $\mathbf{b}_\varepsilon$ is the beam-pointing unit vector with plus or minus one standard deviation error in its components (standard deviations are given in Table 3), $\mathbf{V}_p$ is the aircraft velocity vector in ACRS at the antenna, $\boldsymbol{\varepsilon}_p$ is the aircraft velocity error in ACRS, $k_{s,c}$ is the shear in the weather target velocity across the beam, r is the range to the target (m), and δ_b is the maximum angle between $\mathbf{b}$ and $\mathbf{b}_\varepsilon$ (as given in Table 3).

For the case shown in Fig. 13, the aircraft mean velocity is $\mathbf{V}_p = (61.94, -6.52, 5.33)\,\mathrm{m\,s^{-1}}$ and the assumed velocity error is $0.01\,\mathrm{m\,s^{-1}}$. The calculated maximum error ε is $0.024\,\mathrm{m\,s^{-1}}$, assuming the most unfavorable combination of one standard deviation in the $\mathbf{b}_\varepsilon$ components. The error is very similar for the down–forward beam. The wind shear component $k_{s,c}r\delta_b$ in (3) for this case is negligible. Note that even in the presence of strong shear, this component is always small for radar ranges less than 10 km. For example for $0.01\,\mathrm{s^{-1}}$ shear at 10 km, this component contributes $0.035\,\mathrm{m\,s^{-1}}$. There are other conditions, like low SNR, strong attenuation, and a large contribution from antenna sidelobes (Damiani and Haimov 2006) that can affect the accuracy of a single Doppler radial velocity from weather targets. Among them the SNR has the largest contribution for this example. The minimum detectable signals for the down beam and the down–forward beam, defined as SNR = 0 dB (signal power equal to the noise power), are from −38.5 to −40.0 dBZ and from −33.2 to −35.0 dBZ at 1 km, respectively. Less than 1% of the data from the down and down–forward beam have SNR between 0 and +10 dB and more than 95% of the data have SNR greater than +20 dB. The uncertainty in the weather

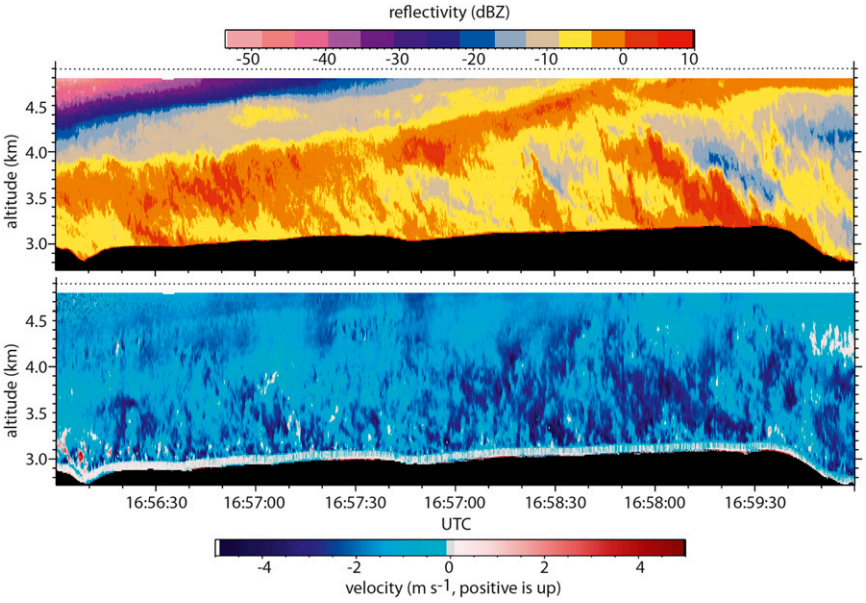

FIG. 13. (top) WCR reflectivity and (bottom) Doppler velocity (corrected for aircraft motion contribution) from down-beam data recorded during UWKA ASCII flight on 19 Jan 2012. UWKA is flying west over the Medicine Bow Mountains in southeastern Wyoming (solid red line, Fig. 11). Dotted line across the top shows the aircraft flight level, and the white band below it is the radar blind zone. The black-filled area across the bottom is a cross section of the terrain.

target Doppler for $0 < \mathrm{SNR} < 10$ dB is greater than 0.5 and less than 2 m s^{-1}, and for SNR ≥ 20 dB it is less than 0.2 m s^{-1}. Overall the uncertainty in the single Doppler hydrometeor motion measurements for the case shown in Fig. 13 is mostly below 0.2 m s^{-1}. Only a small fraction of this uncertainty ($\sim$0.02 m s^{-1}) is caused by the error in the beam-pointing angles and the navigation data.

6. Summary and conclusions

In this paper, by taking advantage of a high-accuracy GNSS-aided inertial geopositioning system, we define the aircraft motion correction of the Doppler velocity measurements as a radar antenna angle calibration problem, described by the nonlinear system (2). To estimate the beam angles, we designed a set of aircraft maneuvers and defined the necessary conditions in order to secure a well-conditioned system (2a). The analysis of the results show that acquiring data from about 30–40 calibration legs in near-optimal environmental conditions is sufficient to retrieve the uncertainty envelope of the radar beam-pointing vector and a good estimate of the calibration coefficients. We also conclude that flying calibration circles only, with roll angles between 30° and 45°, provides the necessary robustness in the solution. For the WCR installation of the down antennas on the UWKA, the uncertainty in the aircraft lateral component of the radar beam unit vectors is relatively large, but it can be reduced significantly by using the constraint (2b). A few pairs of opposite heading straight and level crosswind legs were helpful to perform further fine adjustment in the beam vector.

We also analyzed the individual contributors to the uncertainty in the beam angles. The main causes of errors in the beam angle are the noise in the radar Doppler velocity measurements and the limited decorrelation in time of the platform motion into the radar beam components for some of the legs. Careful examination of the output of the solver of (2) is needed in order to remove legs that cause outliers because of erroneous solutions. Accounting for the radar-arm moment contribution is necessary even for short length (1–2 m) of **R**. However, errors in **R** less than 0.1 m, which are reasonable to achieve with standard surveying techniques, have a negligible effect on the accuracy of the radar-arm moment. The errors in the beam-pointing angles resulting from the airframe distortion are small and overlap with the errors because of solution inaccuracies, at least for the radar installation on the UWKA. One exception is the effect of the changes in the cabin pressurization. For the UWKA this effect can be noticeable when the pressure differential exceeds 300 hPa, but it is relatively small and typically introduces less than 0.1 m s^{-1} bias.

For the two WCR down-pointing antennas on UWKA, the uncertainty envelope is narrow and the rms error in the calibrated down and down–forward beams is smaller

than 0.03°. This error is estimated to contribute less than $0.05\,m\,s^{-1}$ for UWKA speeds near $100\,m\,s^{-1}$, winds of up to 40–$50\,m\,s^{-1}$, downdrafts and updrafts of up to $20\,m\,s^{-1}$, and flight altitudes lower than 7000 m. For the case shown in Fig. 13, the maximum error in the single Doppler velocity due to one standard deviation beam-pointing uncertainty is $0.024\,m\,s^{-1}$. Analysis of the dataset from the ASCII campaign showed that one set of beam calibration coefficients is sufficient for application to the entire dataset.

The described calibration procedure should be applicable to fixed-beam airborne Doppler radars installed on other aircraft. Higher accuracy may be achieved by mounting the IMU/GNSS system as close as possible to the antenna phase center, minimizing the error in the moment arm correction. This might be especially important for radars on aircraft that are subject to larger airframe distortion.

Acknowledgments. The UWKA and WCR are part of the Lower Atmospheric Observing Facilities Program of the National Science Foundation, and are supported under the NSF–University of Wyoming Cooperative Agreement AGS-0832637. The ASCII project was funded under NSF Grant AGS-1058426. The authors are in debt to the UWKA facility staff for the technical support and the operation of the radar, and especially the pilots who did an excellent job during the calibration flights. We are also thankful to Dr. Andrew Pazmany and Dr. Jeffrey French for the useful discussions about this research.

REFERENCES

Applanix, cited 2012: POS AV specifications. Applanix Corp., Richmond Hill, ON, Canada. [Available online at http://www.applanix.com/media/downloads/products/specs/POSAV_SPECS.pdf.]

ASTER, cited 2012: ASTER: Advanced Spaceborne Thermal Emission and Reflection Radiometer. NASA Jet Propulsion Laboratory, California Institute of Technology, Pasadena, CA. [Available online at http://asterweb.jpl.nasa.gov.]

Barton, D., and H. R. Ward, 1984: *Handbook of Radar Measurement.* Artech House, 426 pp.

Bosart, B. L., W. C. Lee, and R. M. Wakimoto, 2002: Procedures to improve the accuracy of airborne Doppler radar data. *J. Atmos. Oceanic Technol.,* **19,** 322–339.

Damiani, R., and S. Haimov, 2006: A high-resolution dual-Doppler technique for fixed multiantenna airborne radar. *IEEE Trans. Geosci. Remote Sens.,* **44,** 3475–3489.

Durden, S. L., Z. S. Haddad, and T. P. Bui, 1999: Correction of Doppler radar data for aircraft motion using surface measurements and recursive least squares estimation. *J. Atmos. Oceanic Technol.,* **16,** 2026–2029.

Georgis, J. F., F. Roux, and P. H. Hildebrand, 2000: Observation of precipitating systems over complex orography with meteorological Doppler radars: A feasibility study. *Meteor. Atmos. Phys.,* **72,** 185–202.

Haimov, S., and A. Rodi, 2012: Beam-pointing angle calibration of the Wyoming Cloud Radar on the Wyoming King Air aircraft. Preprints, *Seventh European Conf. on Radar in Meteorology and Hydrology,* Toulouse, France, Selex-SI and Vaisala, 137 CR. [Available online at http://www.meteo.fr/cic/meetings/2012/ERAD/extended_abs/CR_119_ext_abs.pdf.]

Leon, D., G. Vali, and M. Lothon, 2006: Dual-Doppler analysis in a single plane from an airborne platform. *J. Atmos. Oceanic Technol.,* **23,** 3–22.

NCAR, cited 2012: Electra Doppler Radar (ELDORA). National Center for Atmospheric Research. [Available online at http://www.eol.ucar.edu/rsf/eldora/eldora.html.]

Skolnik, M., 2008: *Radar Handbook*. 3rd ed. McGraw-Hill, 1200 pp.

Testud, J., P. H. Hildebrand, and W.-C. Lee, 1995: A procedure to correct airborne Doppler radar data for navigation errors using the echo returned from the earth's surface. *J. Atmos. Oceanic Technol.,* **12,** 800–820.

UWKA, cited 2012: University of Wyoming King Air Research aircraft (N2UW). University of Wyoming, Laramie. [Available online at http://www.atmos.uwyo.edu/n2uw.]

Wang, Z., and Coauthors, 2012: Single aircraft integration of remote sensing and in situ sampling for the study of cloud microphysics and dynamics. *Bull. Amer. Meteor. Soc.,* **93,** 653–668.

WCR, cited 2012: Wyoming Cloud Radar. University of Wyoming, Laramie. [Available online at http://www-das.uwyo.edu/wcr/.]

Wendisch, M., and J.-L. Brenguier, Eds., 2013: *Airborne Measurements for Environmental Research: Methods and Instruments.* Wiley-VCH, 641 pp.